REPORT DOCUMENTATION PAGE	Form Approved OMB NO. 0704-0188

Public Reporting burden for this collection of information is estimated to average 1 hour per response, including the time for reviewing instructions, searching existing data sources, gathering and maintaining the data needed, and completing and reviewing the collection of information. Send comment regarding this burden estimates or any other aspect of this collection of information, including suggestions for reducing this burden, to Washington Headquarters Services, Directorate for information Operations and Reports, 1215 Jefferson Davis Highway, Suite 1204, Arlington, VA 22202-4302, and to the Office of Management and Budget, Paperwork Reduction Project (0704-0188,) Washington, DC 20503.

1. AGENCY USE ONLY (Leave Blank)	2. REPORT DATE 1 Jul 99	3. REPORT TYPE AND DATES COVERED Final 28 Mar 94 - 31 Mar 99

4. TITLE AND SUBTITLE Effects of Solid-Solid Phase Changes On Impact Mechanics	5. FUNDING NUMBERS DAAH04-94-G-0063

6. AUTHOR(S) T. J. Ahrens, C. Liu, J. K. Knowles, N. S. Brar	

7. PERFORMING ORGANIZATION NAME(S) AND ADDRESS(ES) California Institute of Technology, 252-21 1200 E. California Blvd. Pasadena, CA 91125	8. PERFORMING ORGANIZATION REPORT NUMBER

9. SPONSORING / MONITORING AGENCY NAME(S) AND ADDRESS(ES) U. S. Army Research Office P.O. Box 12211 Research Triangle Park, NC 27709-2211	10. SPONSORING / MONITORING AGENCY REPORT NUMBER ARO 31403.6-EG

11. SUPPLEMENTARY NOTES The views, opinions and/or findings contained in this report are those of the author(s) and should not be construed as an official Department of the Army position, policy or decision, unless so designated by the documentation.	

12 a. DISTRIBUTION / AVAILABILITY STATEMENT Approved for public release; distribution unlimited.	12 b. DISTRIBUTION CODE

DTIC QUALITY INSPECTED 4

19991101 148

13. ABSTRACT (Maximum 200 words)

Stress-wave profiles in vitreous GeO_2 induced by planer and spherical projectile impact were measured using piezoresistance gauges in the 4 to 18 GPa shock pressure range. Comparison of the shock data for fused SiO_2 with those for vitreous GeO_2 demonstrates that range of transformation to a denser, presumably 6-fold coordinated structure in both media are similar. The Hugoniots of GeO_2 and SiO_2, both initially vitreous, are found to be virtually coincident if pressure in SiO_2 is calculated by multiplying the GeO_2 pressure by the ratio of the initial densities of vitreous GeO_2 to fused SiO_2. The volume axes are translated with the specific volumes upon onset and completion of the phase change are aligned. This result, as well as the usual crystal-chemical structural arguments, provides the basis for considering vitreous GeO_2 as an analogous material to fused SiO_2. Our spherical projectile impact results demonstrate: (1) The supported elastic shock in fused SiO_2 decays less rapidly than a linear elastic wave when elastic wave stress amplitude is higher than 4 GPa. A supported elastic precursor in vitreous GeO_2 decays faster with radius than a linear elastic wave; (2) In GeO_2 (vitreous) unsupported shock waves decay with peak pressure in phase transition range (4-15 GPa) with propagation radius (r) as $\propto r^{-3.35}$, close to the prediction of Chen [1999].

14. SUBJECT TERMS	15. NUMBER OF PAGES
GeO_2, shock attenuation, phase change, equation of state	
	16. PRICE CODE

17. SECURITY CLASSIFICATION OR REPORT	18. SECURITY CLASSIFICATION ON THIS PAGE	19. SECURITY CLASSIFICATION OF ABSTRACT	20. LIMITATION OF ABSTRACT
UNCLASSIFIED	**UNCLASSIFIED**	**UNCLASSIFIED**	**UL**

Effects of Solid-Solid Phase Changes On Impact Mechanics

Final Report

T.J. Ahrens
C. Liu
J.K. Knowles
N.S. Brar

June 1999

U.S. ARMY RESEARCH OFFICE

GRANT NO. DAAH04-94-G-0063

California Institute of Technology
Pasadena, CA 91125

Approved for Public Release;
Distribution Unlimited

The views, opinions, and/or findings contained in this report are those of the author(s) and should not be construed as an official Department of the Army position, policy, or decision, unless so designated by other documentation.

Table of Contents

List of Illustrations

List of Tables

ABSTRACT

Stress-wave profiles in vitreous GeO_2 induced by planer and spherical projectile impact were measured using piezoresistance gauges in the 4 to 18 GPa shock pressure range. The planer experiments demonstrate that the response of vitreous GeO_2 to planar shock loading can be divided into three regimes: (1) An elastic shock regime with ramp Hugoniot elastic limit (HEL) precursor with a peak stress and particle velocity of 4 GPa and 0.33 km/s. Its propagation velocity decreases from an initial longitudinal elastic wave speed of 3.5 km/s at essentially zero-amplitude, to 2.8 km/s at 4 GPa; (2) A transition wave regime. Here a ramp wave is superimposed on the precursor with an amplitude of 0 to 2 GPa for peak loading pressures of 8 to 14 GPa. Above 4 GPa the ramp wave velocity decreases to a value below 2.5 km/sec (the speed of the bulk wave, at the HEL); (3) A shock wave achieving the final shock state forms when peak pressure is >6 GPa. This wave can be described via the linear shock-particle velocity relation $D = 0.917 + 1.71\ u$ (km/s) over the 6 – 40 GPa range for an initial density of 3.655 g/cm^3. Combining the Jackson and Ahrens [Jackson and Ahrens, 1979] data and the present demonstrates the phase change from 4- to 6-fold coordination of Ge^{+4} with O^{-2} in GeO_2 occurs in the pressure range of 4 to 15 ± 1 GPa under planar shock loading. Comparison of the shock data for fused SiO_2 with those for vitreous GeO_2 demonstrates that range of transformation to a denser, presumably 6-fold coordinated structure in both media are similar. The Hugoniots of GeO_2 and SiO_2, both initially vitreous, are found to be virtually coincident if pressure in SiO_2 is calculated by multiplying the GeO_2 pressure by the ratio of the initial densities of vitreous GeO_2 to fused SiO_2. The volume axes are translated with the specific volumes upon onset and completion of the phase change are aligned. This result, as well as the usual crystal-chemical structural arguments, provides the basis for considering vitreous GeO_2 as an analogous material to fused SiO_2. Our spherical projectile impact results demonstrate: (1) The supported elastic shock in fused SiO_2 decays less rapidly than a linear elastic wave when elastic wave stress amplitude is higher than 4 GPa. A supported elastic precursor in vitreous GeO_2 decays faster with radius than a linear elastic wave; (2) In GeO_2 (vitreous) unsupported shock waves decay with peak pressure in phase transition range (4-15 GPa) with propagation radius (r) as $\propto r^{-3.35}$, close to the prediction of Chen [1999]. Based on a simple analysis of spherical wave propagation, we find that the different decay rates of a spherical elastic wave in fused SiO_2 and vitreous GeO_2 are predictable on the basis of the magnitude and sign of $\partial K/\partial P_{HUG}$, where K is bulk modulus and P, shock pressure.

INTRODUCTION

In the 1960's and early 1970's when the first shock wave measurements were conducted on silicates [Wackerle, 1962], [Fowles, 1967], [Ahrens and V. G. Gregson, 1964], [McQueen et al., 1967], [Ahrens et al., 1969] it became clear that this class of materials all demonstrated behavior which indicated that transformation to dense structures in which Si^{+4} was coordinated to six O^{-2} ions as in, the then recently discovered, (at Meteor Crater, Arizona) high-pressure phase of SiO_2, stishovite (rutile-structured phase) which has a density of 4.30g/cm^3, some 62% and 95% greater than crystal or fused quartz starting materials [Chao, 1962]. Motivated by scientific curiosity and a need to contain explosive products and understand the interaction with

rock of nuclear explosions in the Earth, a detailed series of measurements of release isotropes of SiO_2 and other silicate minerals shocked into the mixed phase and high pressure phase regime were obtained [Grady et al., 1974], [Podurets et al., 1988], [Chhabildas and Miller, 1985]. All these data point to the general conclusion that transformation to the high-pressure phase occurred upon overdriving the low-pressure phase to a significantly higher shock pressure than required for thermodynamic equilibrium by, in several cases, a factor of two. Upon unloading, the mixed phase and/or high-pressure phase regimes demonstrated hysteretic behavior. This indicates that unloading was occurring in pressure-density plane along the isentrope of the high-pressure phase and, as a result of this hysteresis, the silicates appeared to be extremely absorptive of shock energy, e.g. Swegle [1990]. Only recently have we understood this behavior in terms of the inclusion theory of Truskinovsky [1984], which although developed to describe quasi-static transformation is expected to be applicable to many shock-induced transformations, including the quartz-stishovite transformation [Stolper and Ahrens, 1987] because it is martinsitic in nature as are other major and important phase changes such as the $\alpha \rightarrow \varepsilon$ phase (iron), B1 $\rightarrow$ B2 phase (alkali halides), and graphite $\rightarrow$ diamond.

Although it was long recognized that the phase transformation in silicates and SiO_2 occurred at stress levels of ~10-20 GPa. This stress level and hence these transformations were out of range of interest of light armor materials that are effective against small arms projectiles.

However, in the case of GeO_2 and other germenates this does not seem to be the case. For GeO_2 (which has a phase diagram similar to SiO_2) the glass (3.64 g/cm^3) to rutile-like phase (6.25 g/cm^3) transformation demonstrates a density increase of 72% that occurs over the pressure range of 4-15 GPa. This shock stress range is inferred on the basis of the present work and the early studies of Jackson and Ahrens [Jackson and Ahrens, 1979]. This is the pressure range of interest upon small arms fire striking GeO_2 glass and hence this, in combination with other materials, could possibly be useful as a potential ingredient in a transparent armor system.

In this report we briefly review the previous work on a program initiated in 1996 in which the release isotropes of GeO_2 were first measured and these were used to model excess attenuation in the phase transformation region. Our recent work in which shock structure and attenuation in GeO_2 in one-dimensional longitudinal compression and a spherical diverging shock wave are summarized.

PREVIOUS RESEARCH ON GeO_2

Motivated by the possibility that further coordination increases in ${}^{\chi}M^{+4}O_2$, e.g.

$${}^{VI}M^{+4}O_2 \rightarrow {}^{VII}M^{+4}O_2 \rightarrow {}^{VIII}M^{+4}O_2$$

where χ is a 6-, 7-, or 8-fold coordination of a metal ion (M) in column 4A of the periodic table (M = Si, Ge, Sn, Pb) or in column 4B (M = Ti, Zn, Hf, Rf), Jackson and Ahrens [1979] studied

shock compression of GeO_2 both in vitreous (4-fold coordinated) and in rutile (6-fold coordinated) structures to determine whether further transformation occurred.

The column 4 elements mentioned above actually achieve a number of structures and several that have higher coordination than 6. These have been studied and classified by J.M. Leger [1996]. The Hugoniot data for GeO_2 is plotted in Figure 1 together with the static compression data for GeO_2, starting from glass and quartz structure. Also, GeO_2 in the quartz phase transforms to a vitreous phase upon recovery from dynamic compression to 7 GPa whereas SiO_2 demonstrates this behavior at >15 GPa under both static and dynamic compression [Kingma et al., 1995]. As shown in Figure 1, transformation of a dense rutile-like structure (6.3 g/cm^3) begins at ~4 GPa and is complete at ~15 GPa. The shock velocity-particle velocity plane, Figure 2, explicitly demonstrates that the pressure range of transformation corresponds to particle velocities in the 300-800 m/s range. This velocity range corresponds to particle velocities imparted by small arms fire projectiles striking GeO_2 glass.

Earlier motivated by the substantial increase in density displayed by Hugoniot curves, Chen et al. [1999] measured the release isentropes in order to allow calculation of the excess energy deposited in the GeO_2 in regions where the vitreous to rutile structure phase change occurred. It was expected that this hysteretic phase change could result in severe attenuation in the amplitude of an unsupported diverging shock as it decays through the 14 to 4 GPa range. At lower stresses the attenuation is expected to be no longer anomalous. In silicate-igneous and carbonate and other sedimentary rock types, the attenuation rate when fit to a power law indicate the shock stress σ_H decays with radius directly beneath a point source at the surface as:

$$\sigma_H \propto 1/r^n$$

where n varies from 1.5 to 1.8 for $\sigma_H \sim$ 2-300 GPa. [Ahrens and O'Keefe, 1985]. The attenuation rate from fully contained explosions over a similar stress range is similar with n = 1.7 – 1.8 [Cooper, 1977].

The release isentropes (Figure 1b) for GeO_2 glass were measured using the experimental setup of Figure 4. In the two forward experiments (Figure 4a) 3-4 mm thick samples were impacted at 1.5 and 2.0 km/sec with 2.6 mm thick tungsten plates (Table 1). In the reverse experiments (Figure 4b) 3 or 4 mm thick plates of GeO_2 were launched at 0.8 to 1.5 mm thick 6061 Al buffer plates at speeds of 0.6 to 2.0 km/sec.

A typical VISAR record is shown in Figure 5a (this was a forward shot). The wave profile with a 14 GPa amplitude displays a 0.6 GPa elastic precursor and is fit with a hysteretic model to produce Figure 5c. Panel 5b was calculated using the standard Gruneiser equation-of-state but lacking a hysteretic equation of state. The peak pressure duration that is calculated is clearly much longer than observed in Figure 5a. The numerical simulations shown were performed with the one-dimensional compressible flow computer code, WONDY [Kipp and

Lawrence, 1982]. We compare calculated profiles to those measured with the VISAR to yield a series of release isentropes that are shown in Figure 1b. Only the initial release isentropes actually are well defined by the VISAR data. The initial unloading is induced by the arrival of a rarefaction wave from the rear of the flyer plate in both forward and reverse configuration (Figure 4a,b). The particle velocity profiles are useable until arrival of lateral rarefaction waves at the VISAR reflection point in the center of the sample about 0.5 μs after the initial rarefaction wave from the rear of the flyer plate attenuates the peak shock pressure.

Using the release isentropes of Figure 1b for the phase transition region, Chen et al. [, 1998 #3783] calculates the stress wave attenuation for the geometry of Figure 6. We approximate the stress attenuation from a projectile striking a target by examining the stress wave decay from a spherical flyer plate impacting a sample in radial geometry. The peak stress wave decrease with propagation radius is shown in Figure 7 for both reversible and irreversible unloading model. It is clear that more rapid decay of peak stress amplitude with radius takes place in the pressure regime of the hysteretic phase change. The shock pressure from the spherical source (which is a model of the stress attenuation along the centerline beneath a normal projectile impact on a GeO_2 half space) was predicted to decay in Chen et al. [, 1998 #3783] with a power-law (Equation 1) with n = 2.71. This is considerably more attenuative than the regimes where the phase change does not occur. We point out that analogous behavior over the shock stress range 9-30 GPa in SiO2 were calculated for radial flow by Swegle [1990] although these results were not fit to a power-law curve.

PLANE-WAVE PROPAGATION IN GeO_2

Using Manganin gauges, in planar flow geometry, we conducted measurements of elastic precursor decay from final shock states in the range of 8-16 GPa using the geometry of Figure 9. Previously Wackerle [1962] measured elastic precursor decay in fused quartz. Because the fused quartz elastic Hugoniot is convex upward in the pressure-volume phase to 6 GPa the initial portion of the SiO_2 glass precursor are dispersive. However, at stresses above the 6 GPa level a normal steep shock front is induced because the Hugoniot becomes concave downward. This occurs up to the Hugoniot elastic limit (HEL) of 9 GPa. Thus SiO_2 can be viewed as displaying a partially supported elastic precursor. We find that, as expected, this wave decay occurs slowly with distance and goes with n = 0.54. In contrast, the elastic precursor in GeO_2, which is always dispersive up to the 4 GPa (Figure 10), decays more rapidly with n = 1.24 (Figure 11).

SPHERICAL WAVE DECAY

We have only fired two experiments that unequivocally demonstrated unsupported wave decay in spherical geometry using the set-up shown in Figure 12. As a result of the radial flow induced by the spherical impactor the manganin gauge resistance (50 ohms-Dynasen-MN4-50) increases as a result of both stretching as a result of the radial diverging flow and a result of being encompassed by the increasing shock stress. To take this into account, we employ also in the same planes, Constantan strain gauges (MN/CN-4-50-ER Dynasen). Constantan alloy is

relatively insensitive to shock heating. However, like Manganin, it suffers stretching when placed perpendicular to a radial flow.

We combined data from Manganin and Constantan and employed the latter to apply a stretching correction to the Manganin record, for example, Figure 13. Spherical elastic precursor decay for one experiment is shown in SiO_2 in Figure 14 and vitreous GeO_2 in Figure 15. An approximate fit to the GeO_2 data, taking into account a region 0.2 X_o in radius (X_o is the spherical impactor radius of Figure 11). In this close-in (region A), Figure 15, $0<x/X_o<0.2$ the stress wave attenuation is slight as the flow is nearly planar and only a slight deviance of stress occur with increasing radius (due to the slightly diverging flow). This feature of shock attenuation from impact was observed by Ahrens and O'Keefe [1977] (Figure 16).

In Region B (Figure 15) the shock attenuation is dominated by the hysteretic phase transition and a decay rate of N=3.35 is estimated in Figure 17.

CONCLUSIONS

The stress wave attenuation from spherical unsupported shocks in engineering and geologic materials yield stress wave decay exponents of n = 1.5 to 1.8 (Equation 1) in the 0.5 to 150 GPa pressure range. The present data are consistent with hysteretic behavior associated with n~3. We calculate a value of n = 3.35 on the basis of two spherical experiments within the phase transition region with virtually no control of uncertainty. This compares to the n = 2.7 predicted exponent [Chen, 1998 #3783] in this stress range. GeO_2 appears to be representative of a hysteretic phase change materials and would appear to be extremely attenuative in the 4-15 GPa phase change regime. Further work on a longer time scales and their effect on ballistic penetration must still be studied.

ACKNOWLEDGEMENT

The release isentrope measurements summarized were initiated by former California Institute of Technology graduate student Wenbo Yang and these data were applied to a numerical simulation of shock attenuation by George Chen. We appreciate the technical support of P. Gelle, M. Long and A. Devora. Research supported by Army Research Office and NASA. Contribution, Division of Geological and Planetary Science, California Institute of Technology.

PUBLICATIONS AND TECHNICAL REPORTS

Publications

1. Knowles, J. K., N. Winferee and T. J. Ahrens. Dynamically induced phase transition and the modeling of comm in brittle solids. *Math and Mech. Solids*, 2, pp. 99-116, 1997.

2. Chen, C. Q., T. J. Ahrens, W. Yang and J. K. Knowles. Effect of irreversible phase change on shock wave propagation. *J. Mech. Phys. Solids*, *47*, 763-783, 1999.

3. Liu, C., T. J. Ahrens and N. S. Brar. Effect of phase change on shock wave attenuation. *Pior. 15th U.S. Army Mech. Conf.*, in press, 1999

4. Liu, C., T. J. Ahrens and N. S. Brar. Effect of phase change on shock wave attenuation. to be submitted to *J. Mech. Phys. Solids*.

5. Knowles, J. K., N. A. Winfree and T. J. Ahrens. Effects of solid-solid phase changes on impact mechanics. *20th International Symposium on Shock Waves*, 1995

Theses

1. Nancy A. Winfree, Impact-induced phase transformations in elastic solids. 1999
   abstract is Appendix A
2. C. Liu, Part II: GeO_2 Phase Change Effect, pp. 135-183, 1999.
   abstract is Appendix B

PARTICIPATING SCIENTIFIC PERSONNEL

T. J. Ahrens

J. K. Knowles

N. A. Winfree

C. Liu

N. S. Brar (U. of Dayton Res. Inst.)

W. Yang

G. Q. Chen

REPORT OF INVENTIONS

n/a

TABLES AND FIGURES

Table 1
VISAR experiments on GeO_2
1. Forward shots

	Flyer plate (Tungsten)		Stationary plate (GeO_2)		Buffer (A16061)
Shot No.	Thickness (mm)	Velocity (km/s)	Thickness (mm)	Density (Mg/m^3)	Thickness (mm)
953	2.627 ±0.003	1.53 ±0.04	3.835 ±0.002	3.632 ±0.002	0.743 ±0.006
955	2.645 ±0.001	1.99 ±0.05	4.059 ±0.002	3.631 ±0.003	0.923 ±0.001

2. Reverse shots

	Flyer plate (GeO_2)			Driver plate (A16061)
Shot No.	Thickness (mm)	Velocity (km/s)	Density (Mg/m^3)	Thickness (mm)
957	4.087 ±0.001	1.47 ±0.05	3.630 ±0.04	1.459 ±0.001
958	4.128 ±0.001	1.96 ±0.08	3.633 ±0.03	1.354 ±0.001
965	3.029 ±0.001	0.62 ±0.01	3.618 ±0.03	0.774 ±0.001

Densities of tungsten and A16061 are 19.2 and 2.70 Mg/m^3, respectively

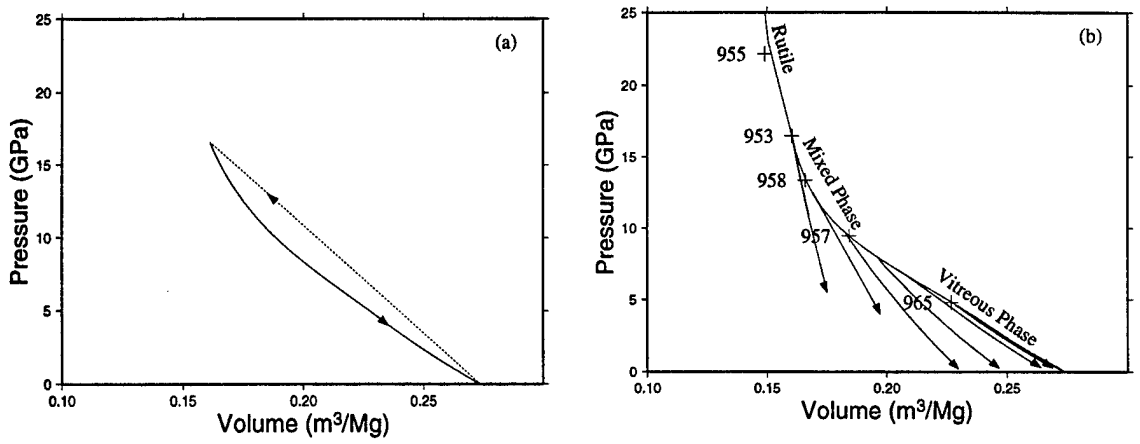

Figure 1. Hugoniots and release isentropes for: (a) reversible phase change models; (b) irreversible (several measured releases at different pressures are shown). For reversible model, release are not distinguishable from Hugoniot. "Waste heat" is area between the Rayleigh line (dashed) and the solid curve release isentrope induces normal attenuation. The hysteretic behavior of Hugoniot-release isentrope loop in (b) enhances dissipation of shock energy and gives rise to increased attenuation.

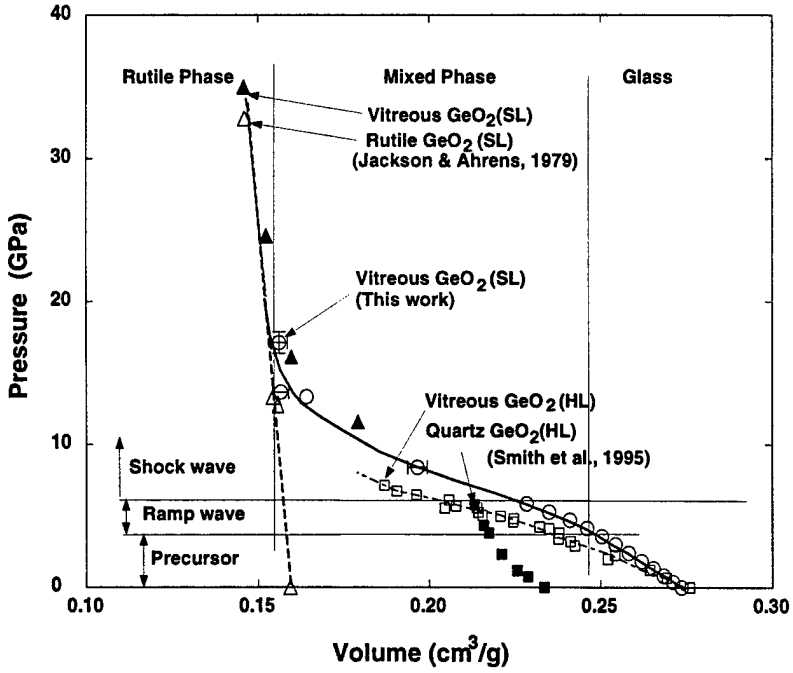

Figure 2. Shock pressure versus volume of vitreous GeO_2. SL and HL are Hugoniot states shock compression and isothermal (hydrostatic) compression states, respectively.

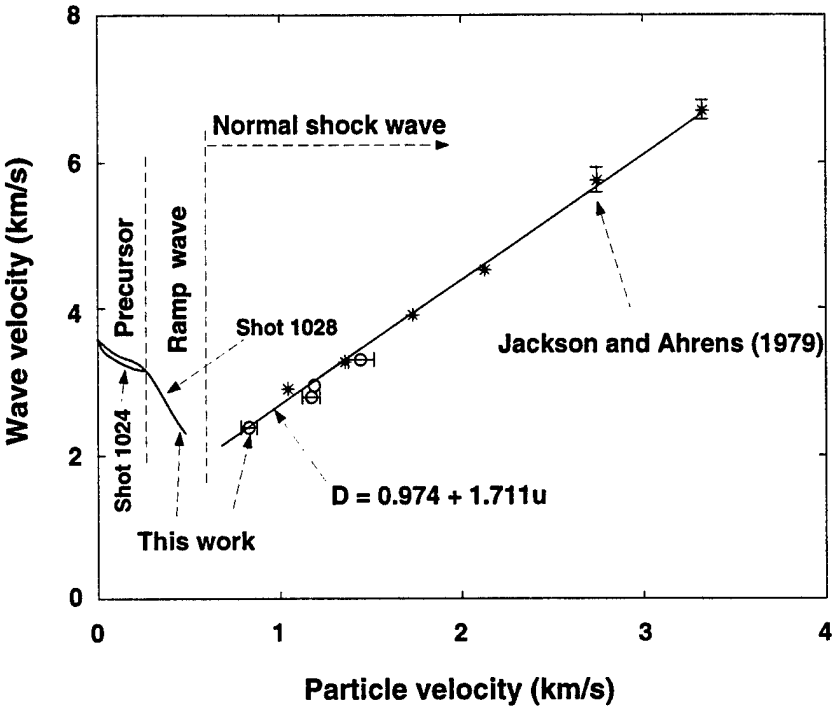

Figure 3. Shock wave versus particle velocity, vitreous GeO_2, initial density.

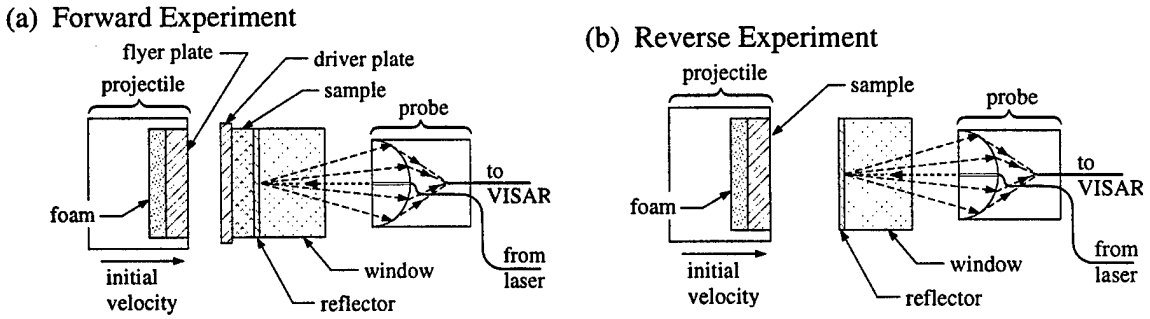

Figure 4. Diagram of GeO_2 release isentrope experiments: (a) Metal flyer plate impacts sample assembly and generates a shock wave through the sample. The rearward propagating shock wave upon passing through the flyer plate reflects the flyer foam interface and propagates forward as a rarefaction wave. VISAR probe detects particle velocity change at aluminum reflector-window interface due to shock and following rarefaction waves. (b) Reverse experiment is similar, except the flyer plate is the sample under study (GeO_2), and it directly impacts the buffer/reflector. Reverse experiments usually provide continuous release data to lower pressures, but GeO_2 is prone to damage during projectile launch.

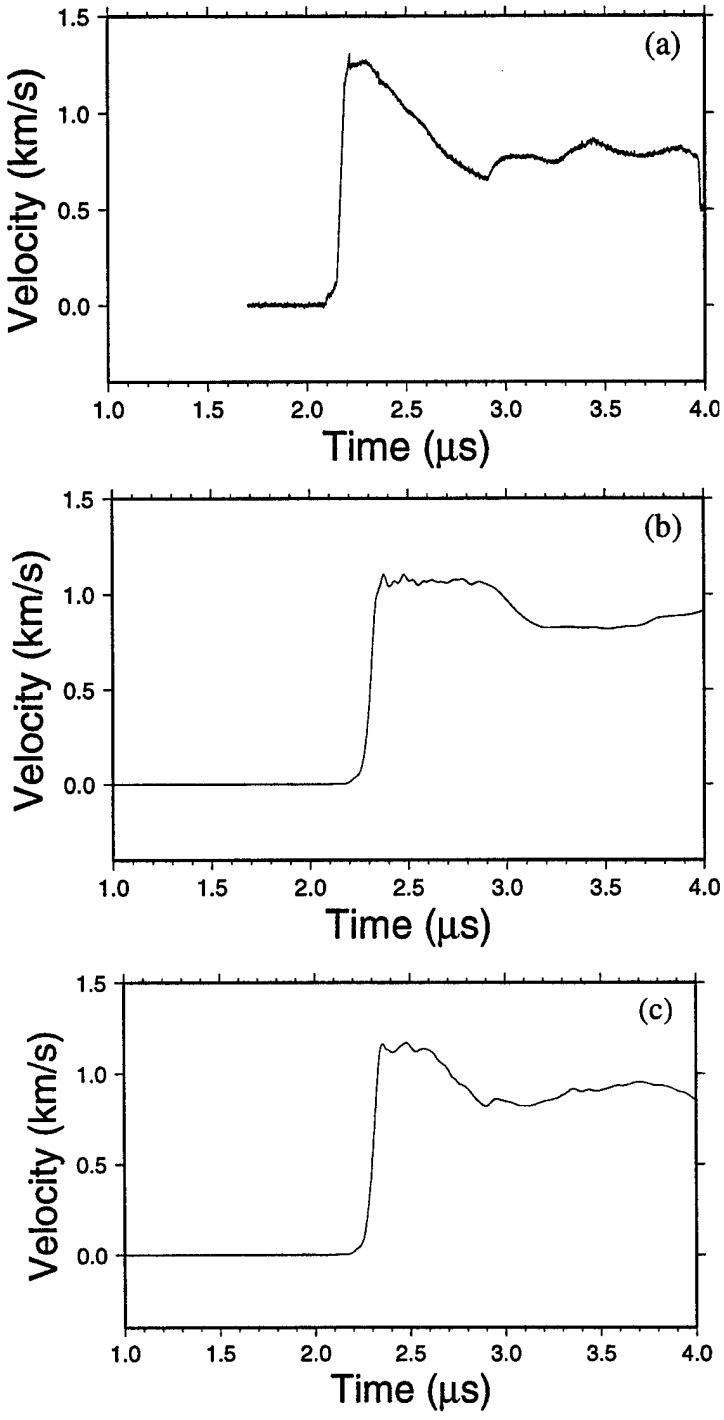

Figure 5. Particle velocity versus time measured by VISAR (a) and calculated (b,c); (b) WONDY fit experiment using a reversible phase change model; (c) WONDY fit to experiment using an irreversible phase change model.

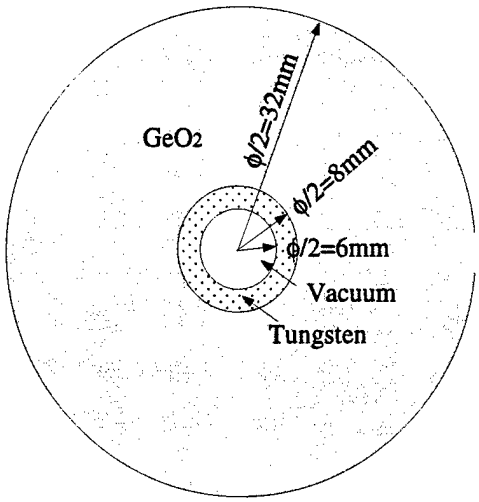

Figure 6. Configuration for calculating shock wave decay in spherical geometry. At time zero, tungsten core impacts surrounding GeO_2 at 1.5 hr/sec simulating impact at surface of a half-space.

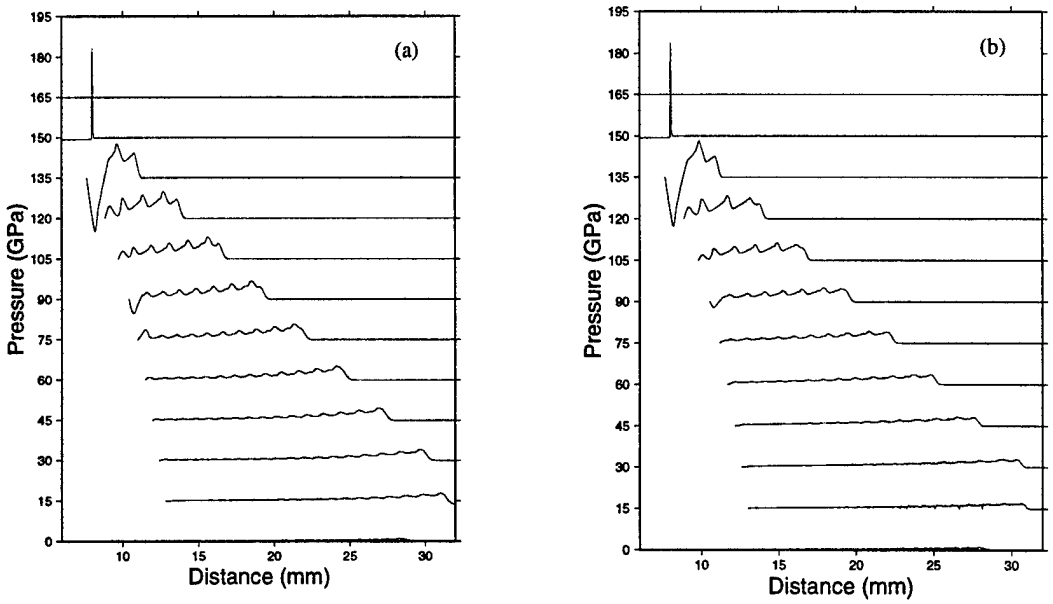

Figure 7. Shock-wave profiles at a series of times (separated by 1 μ sec) in spherical symmetry: (a) Reversible model; (b) Irreversible model. In geometry of Figure 6. Impactor: tungsten, radius from 6 to 8 mm, moving at 1.5 km/s; target: GeO_2 (reversible model), 24 mm thick.

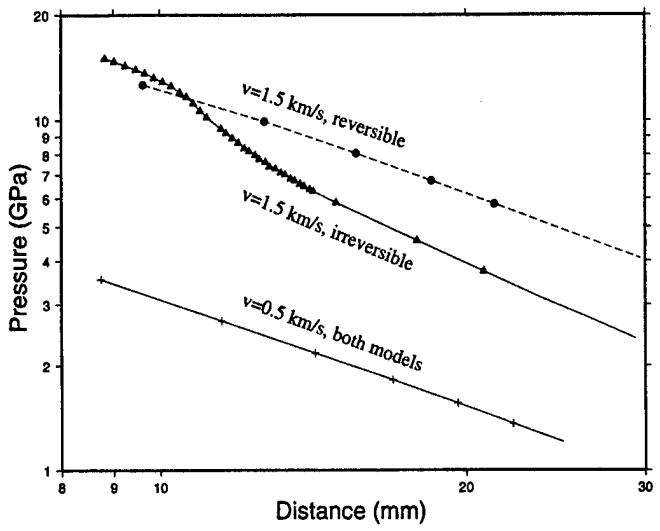

Figure 8. Log_{10} shock-wave amplitude versus log_{10} radius (spherical symmetry). Results for reversible and irreversible models are shown, each with impact velocities of 0.5 km/s and 1.5 km/s. Only 1.5 km/s, with hysteretic behavior results in excess stress wave attenuation over 15 to 4 GPa range.

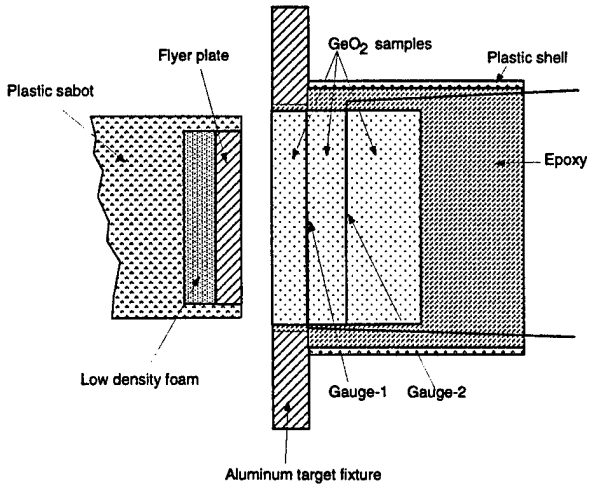

Figure 9. Configuration for propagation experiments in one-dimensional planar flow in the GeO_2 glass. Flyer plate material is 2024 Al or Cu with thickness 4 to 6 mm. Manganin stress gauges are from Dynasen, Inc. Ramp elastic, deformation and also release states are calculated from shock particle and shock propagation velocity and Riemann integral relation. $\sigma(t) = A_0 + A_1 dR(t) + A_2 dR^2(t) + A_3 dR^3(t) + A_4 dR^4(t)$ [Rosenberg et al., 1980]. Here $dR(t)=R(t)-R_0)/R_0(R(t)$ is gauge resistivity during loading at time t and R_0 is initial gauge resistivity. Pressure is calculated from measured voltage change using calibration constant A_i. When $\sigma \leq 1.5$ GPa, $A_1=50$ (GPa) and other coefficients are zero. When $\sigma \geq 1.5$ GPa, $A_0 =$ 0.572 GPa, $A_1=29.59$ GPa/ohm-m, $A_2=95.20$ GPa/(ohm-m)^2, $A_3=312.74$ GPa/(ohm-m)^3 and $A_4=331.77$ GPa/(ohm-m)^4.

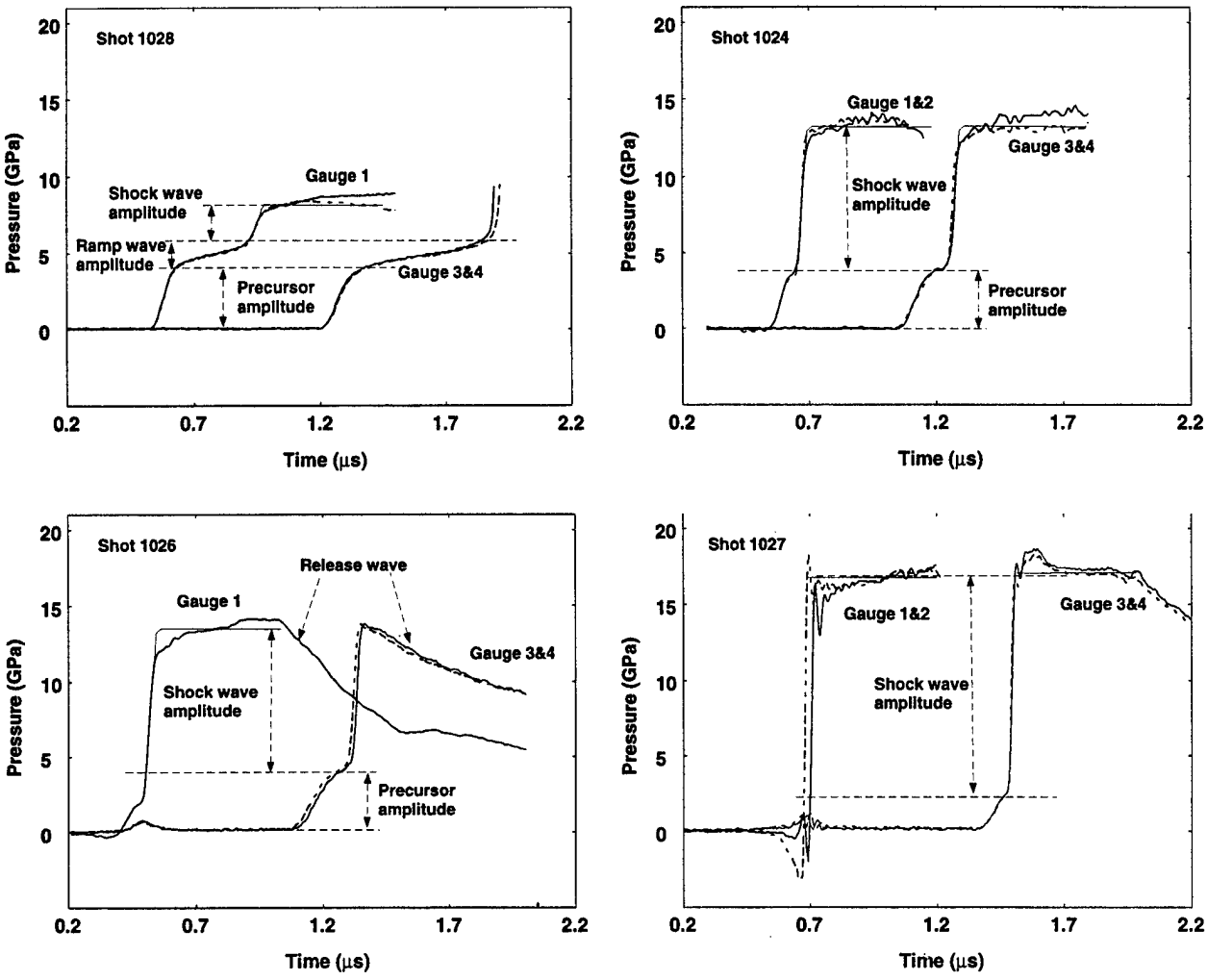

Figure 10. Plane-shock and release wave profiles in vitreous GeO_2 development of 4 GPa elastic precursor with ramp structure is consistant with convex upward elastic Hugoniot.

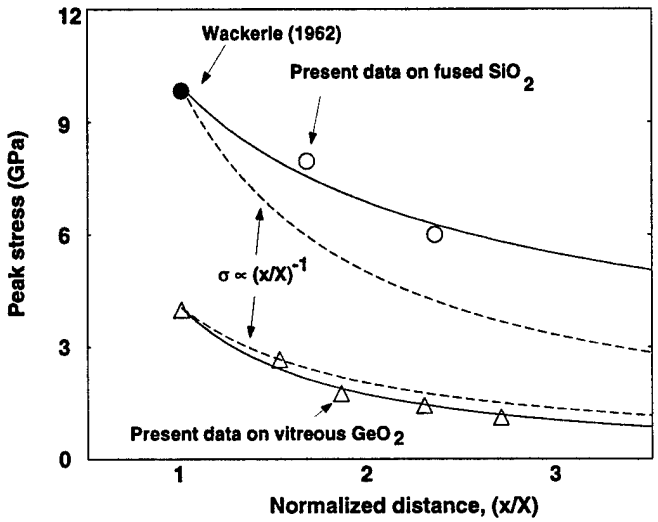

Figure 11. Hugoniot elastic shock amplitude versus normalized propagation distance for vitreous SiO_2 and GeO_2. Normalization distance is initial thickness of flyer plate.

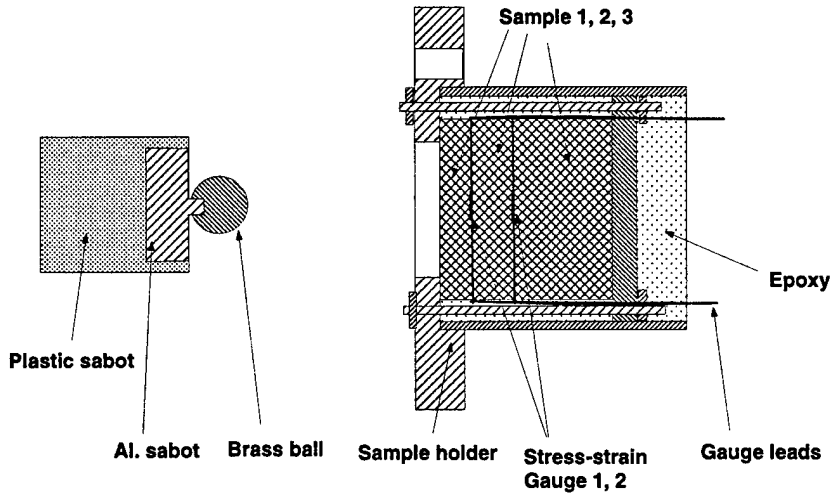

Figure 12. Diagram of spherical impactor radial wave attenuation experiment. Each gauge position incorporates both a Manganin gauge (sensitive to shock pressure and stretching due to radial flow) and a Constantan strain gauge which measures stretching arising from radial flow.

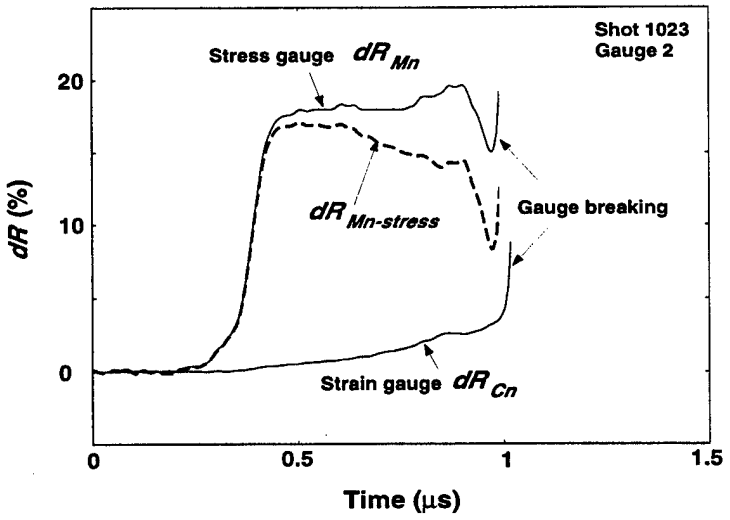

Figure 13. Stress wave profiles in spherically diverging flow. Manganin stress gauge detects increasing resistance with time. Signal is superposition of increased resistance from increase in pressure of shock plus stretch of manganin gauge produced by (lateral) strain parallel to spherical wave front. Lateral strain is measured using a Constantin strain gauge. The Constantin strain gauge record allows correction of stress gauge (Manganin) signal so as to take into account stretching.

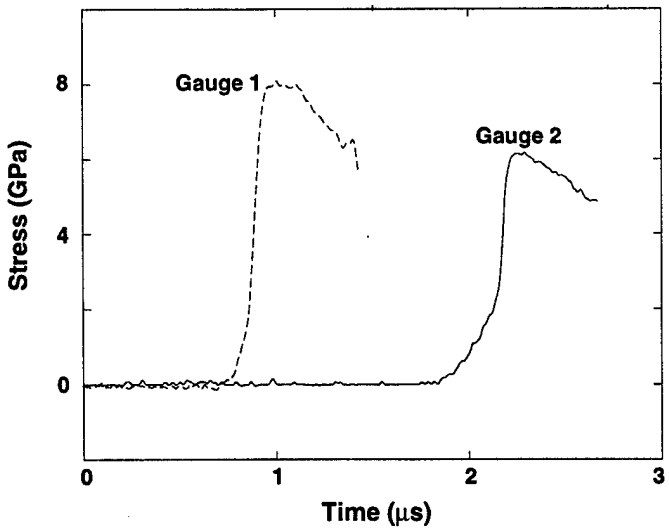

Figure 14. Stress-wave profiles for spherical impact in fused SiO_2. Peak stress measured is approximately at amplitude of Hugoniot elastic limit. Hence observed data give a measure of unsupported elastic shock attenuation in fused SiO_2.

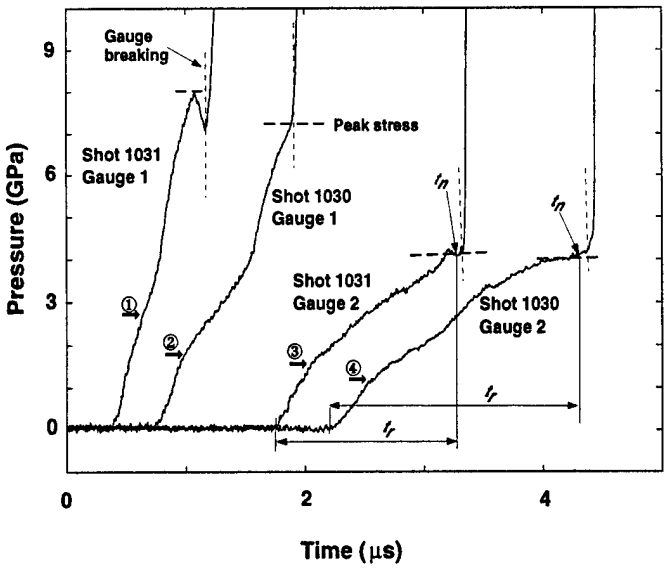

Figure 15. Stress-wave profiles for spherical impactor in vitreous GeO_2. Arrows indicate the amplitude of the precursor originating from impact surface. Note the peak stress decays for 8 to 4 GPa over a 3 mm increment in radius.

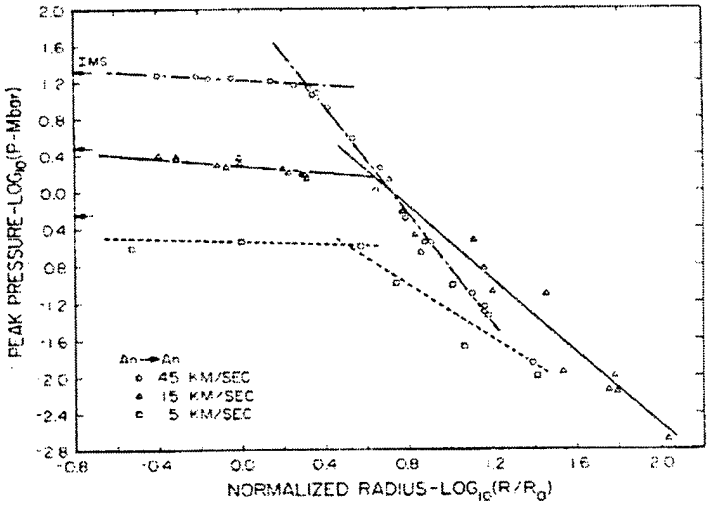

Figure 16. Log_{10} (peak shock presure) versus log_{10} (normalized radius) at various impact velocities for gabbroic anorthosite impactors. Arrows indicate one-dimensional flow pressures. Close in region that has minor attenuation results from a quasi-planar flow (Regime A of Figure 17). Minor divergence of flow induces minor stress wave decay immediately beneath striking projectile (after Ahrens & O'Keefe 1977)

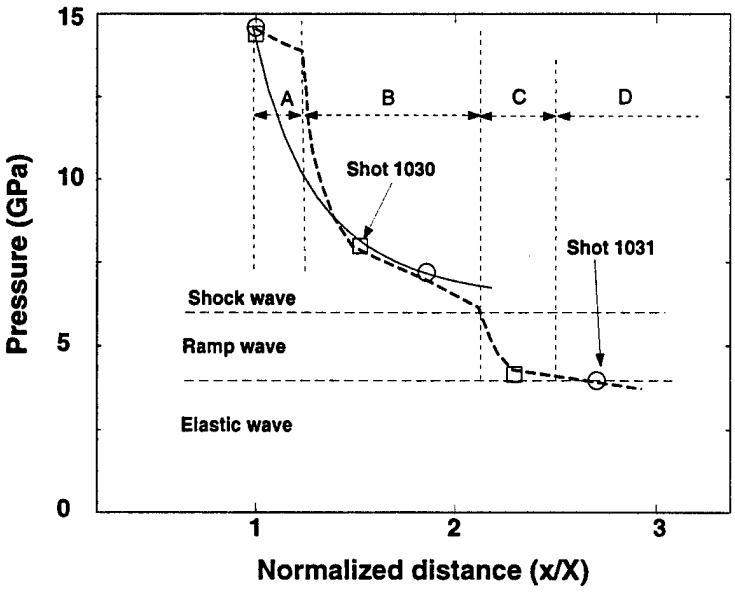

Figure 17. Peak shock pressure versus propagation distance A: near field attenuation. B: phase transition dominated decay. Here peak stress decay is $1/r^n$ where n = 3.35. C: ramp-wave dominated decay. D: elastic-wave decay.

BIBLIOGRAPHY

Ahrens, T. J., and J. D. O'Keefe, Equation of state and impact-induced shock-wave attenuation on the Moon, in *Impact and Explosion Cratering*, edited by D. J. Roddy, et al., pp. 639-656, Pergamon, New York, 1977.

Ahrens, T. J., and J. D. O'Keefe, Shock vaporization and the accretion of the icy satellites of Jupiter and Saturn, in *Ices in the Solar System*, edited by J. Klinger, et al., pp. 631-654, D. Reidel Publishing Company, 1985.

Ahrens, T. J., C. F. Peterson, and J. T. Rosenberg, Shock compression of feldspars, *J. Geophys. Res.*, *74*, 2727-2746, 1969.

Ahrens, T. J., and J. V. G. Gregson, Shock compression of crustal rocks: data for quartz, calcite, and plagioclase rocks, *J. Geophys. Res.*, *69*, 4839-4874, 1964.

Chao, E. C. T., Stishovite, SiO_2, a very high pressure new mineral from Meteor Crater, Arizona, *J. Geophys.*, *92*, 419-421, 1962.

Chen, G. Q., T. J. Ahrens, W. Yang, and J. K. Knowles, Effect of irreversible phase change on shock-wave propagation, *J. Mech. Phys. Solids*, *47*, 763-783, 1999.

Chhabildas, L. C., and J. M. Miller, Release-adiabat measurements in crystalline quartz, SAND 85-1092, Sandia National Laboratory, Albuquerque, N.M., 1985.

Cooper, H. F., Jr., A summary of explosion cratering phenomena relevant to meteor impact events, in *Impact and Explosion Cratering*, edited by D. J. Roddy, et al., pp. 11-44, Pergamon Press, 1977.

Fowles, R., Dynamic compression of quartz, *J. Geophys. Res.*, *72*, 5729-5742, 1967.

Grady, D. E., W. J. Murri, and G. R. Fowles, Quartz to stishovite: Wave propagation in the mixed phase region, *J. Geophys. Res.*, *79*, 332-338, 1974.

Jackson, I., and T. J. Ahrens, Shock-wave compression of vitreous and rutile-type GeO_2: A comparative study, *Phys. Earth Planet. Int.*, *20*, 60-70, 1979.

Kingma, K. J., R. E. Cohen, R. J. Hemley, and H.-K. Mao, Transformation of stishovite to a denser phase at lower-mantle pressures, *Nature*, *374*, 243-245, 1995.

Kipp, M. E., and R. J. Lawrence, WONDY V - A one-dimensional finite-difference wave propagation code, SAND 81-0930, Sandia Natl. Lab., Albuquerque, NM, 1982.

Leger, J. M., J. Haines, M. Schmidt, J. P. Petitet, A. S. Pereira, and J. A. H. daJornada, Discovery of hardest known oxide, *Nature*, *383*, [6599], 401-401, 1996.

McQueen, R. G., S. P. Marsh, and J. N. Fritz, Hugoniot equation of state of twelve rocks, *J. Geophys. Res.*, *72*, 4999-5036, 1967.

Podurets, M. A., G. V. Simakov, and R. F. Trunin, Shock compressibility of quartz mixed with aluminum, *Izvestiya, Earth Physics*, *24*,, 267-270, 1988.

Stolper, E. M., and T. J. Ahrens, On the nature of pressure-induced coordination changes in silicate melts and glasses, *Geophys. Res. Lett.*, *14*, 1231-1233, 1987.
Swegle, J. W., Irreversible phase transition and wave propagation in silicate materials, *J. Appl. Phys.*, *68*, 1563-1579, 1990.
Truskinovskiy, L. M., The equilibrium between a spherical nucleus and the matrix in a solid-state transformation, *Geokhimiya (English translation)*, *3*, 443-447, 1984.
Wackerle, J., Shock-wave compression of quartz, *J. Appl. Phys.*, *33*, 922-937, 1962.

Impact-induced phase transformations in elastic solids: a continuum study including numerical simulations for GeO_2

Thesis by
Nancy A. Winfree

In Partial Fulfillment of the Requirements
for the Degree of
Doctor of Philosophy

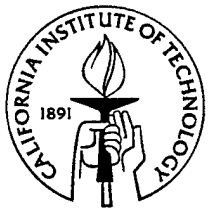

California Institute of Technology
Pasadena, California

1999

(Defended May 13, 1999)

Impact-induced phase transformations in elastic solids: a continuum study including numerical simulations for GeO_2

by

Nancy A. Winfree

In Partial Fulfillment of the
Requirements for the Degree of
Doctor of Philosophy

Abstract

This thesis applies recently developed continuum theories of diffusionless phase transformations in solids to the study of impact problems involving materials which can experience such phase changes. Our objective is to compare the theoretical predictions against certain experimental results.

In the experiments of interest, a face-to-face impact occurs between a disk of amorphous germanium dioxide and another material, either tungsten or an aluminum alloy. The GeO_2 is believed to transform to another phase if sufficient compressive stress is achieved.

We model these experiments using one-dimensional finite elasticity. Phase-changing materials are represented by non-convex potential energy functions. This can produce phase boundaries that propagate *subsonically* or *supersonically* with respect to the slower longitudinal wave speed of the two phases. When a subsonic phase boundary is possible, it is not uniquely determined by the fundamental field equations and jump conditions. Uniqueness is obtained by invoking a *nucleation criterion* to control the initiation of the new phase, and a *kinetic relation* to govern

its evolution.

The experiments considered here are sufficiently long in duration (≈ 3 μs) that several reflections and wave interactions occur, and the analysis becomes analytically intractable. Accordingly, a finite-difference method of Godunov type is employed to analyze these experiments numerically. Methods of Godunov type treat adjoining discretized spatial elements as the two sides of a Riemann problem, which is typically solved *approximately* by linearizing around the initial conditions on each side. Fortuitously, all constitutive models employed in this thesis are such that the required Riemann problems can be solved *exactly* without too much effort.

Simulations utilizing the numerical method demonstrate that the impact response of a material is sensitive to the kinetic relation that enters the model. It appears the theory may offer a plausible description of the experiments, though the restrictions placed on the constitutive models herein seem too severe to provide a good quantitative match to the experimental results.

I Rigid Body Penetration Dynamics

II GeO_2 Phase Change and Its Effect

Thesis by

Cangli Liu

In Partial Fulfillment of the Requirements

for the Degree of

Doctor of Philosophy

California Institute of Technology

Pasadena, California

1999

(Submitted)

Abstract

Stress wave profiles in vitreous GeO_2 were measured using piezoresistance gauges in the pressure range of 5 to 18 GPa under planar plate and spherical projectile impact. Experimental data show that the response of vitreous GeO_2 to planar shock loading can be divided into three stages: (1) A ramp elastic precursor has peak amplitude of 4 GPa and peak particle velocity of 333 m/s. Wave velocity decreases from initial longitudinal elastic wave velocity of 3.5 km/s to 2.9 km/s at 4 GPa; (2) A ramp wave with amplitude of 2.11 GPa follows the precursor when peak loading pressure is 8.4 GPa. Wave velocity drops to the value below bulk wave velocity in this stage; (3) A shock wave achieving final shock state forms when peak pressure is $>$ 6 GPa. The Hugoniot relation is $D = 0.917 + 1.711u$ (km/s) using present data and the data of *Jackson and Ahrens* [1979] when shock wave pressure is between 6 and 40 GPa for $\rho_0 = 3.655$ g/cm^3. Based on the present data, the phase change from 4-fold to 6-fold coordination of Ge^{+4} with O^{-2} in vitreous GeO_2 occurs in the pressure range of 4 to 15 $\pm$ 1 GPa under planar shock loading. Comparison of the shock loading data for fused SiO_2 to that on vitreous GeO_2 demonstrates that transformation to the rutile structure in both media are similar. The Hugoniots of vitreous GeO_2 and fused SiO_2 are found to coincide approximately if pressure in fused SiO_2 is scaled by the ratio of fused SiO_2 to vitreous GeO_2 density. This result, as well as the same structure, provides the basis for considering vitreous GeO_2 as an analogous material to fused SiO_2 under shock loading. Experimental results from the spherical projectile impact demonstrate: (1) The supported elastic shock in fused SiO_2 decays less rapidly than a linear elastic wave when elastic wave stress amplitude is higher than 4 GPa. The supported elastic shock in vitreous GeO_2 decays faster than a linear elastic wave; (2) In vitreous GeO_2, unsupported shock waves decays with peak pressure in the phase transition range (4 -15 GPa) with propagation distance, x, as $\propto 1/x^{-3.35}$, close to

the prediction of *Chen et al.* [1998]. Based on a simple analysis on spherical wave propagation, we find that the different decay rates of a spherical elastic wave in fused SiO_2 and vitreous GeO_2 is predictable on the base of the compressibility variation with stress under one-dimensional strain condition in the two materials.